Exact Wavefield Extrapolation for Elastic Reverse-time Migration

We 02 02

Exact Wavefield Extrapolation for Elastic Reverse-time Migration

M. Ravasi* (University of Edinburgh) & A. Curtis (University of Edinburgh)

SUMMARY

A fundamental step of any wave equation migration algorithm is represented by the numerical projection of the recorded data down into the subsurface where reflections occur. The geophysical community refers to this concept as wavefield extrapolation and the extrapolated wavefield is called the receiver wavefield.

In elastic reverse-time migration, standard wavefield extrapolation only uses partial information contained in elastic waves, and artificial wave energy is extrapolated as a consequence, polluting seismic images.

We propose an exact extrapolation formula, which fully employs the velocity-stress nature of the elastic wavefield to create an improved estimate of the extrapolated receiver wavefield. A synthetic example illustrates the resulting improvements in imaging, providing evidence of the importance of using the full recorded data.

Introduction

Elastic reverse-time migration (ERTM) (Chang and McMechan, 1987; Yan and Sava, 2008) is a promising tool to achieve high resolution imaging in complex geological settings (Lu et al., 2009): it is based on the full elastic wave equation and, in principle, does not require any single-scattering approximation. A central component of ERTM is receiver-side wavefield back-extrapolation in which the scattered wavefield between a physical source and any image point in the subsurface is estimated by projecting the data acquired by receivers located near or at the Earth's surface down into the subsurface.

The commonly-used approximate extrapolation formula involves only particle velocity data and backpropagators. This results in two types of non-physical waves in the scattered wavefield estimate. Here we formulate an exact integral expression for receiver-side wavefield back-extrapolation based on reciprocity theory that uses a combination of velocity-stress recordings and backpropagation sources. It can be further shown that 4-component ocean-bottom cable data provide sufficient information to use this new approach.

A synthetic example is used to compare these different wavefield extrapolation procedures. It explains why artifacts are present in final images when the approximate wavefield extrapolation is carried out, as is usual in elastic reverse-time migration. No such artifacts arise with the new approach.

Elastic receiver-side wavefield extrapolation

Building on the theory of reciprocity and representation theorems for elastic media (Wapenaar and Fokkema, 2006), an exact integral expression for elastic receiver-side wavefield extrapolation from a physical source $\mathbf{x}_s$ to any image point $\mathbf{x}$ is given by:

$$\begin{aligned}\bar{\Phi}_M^S(\mathbf{x},\mathbf{x}_s) = &-\int_{\partial V_r}\left(\tau_{ij}^S(\mathbf{x}_r,\mathbf{x}_s)\left\{G_{(M,i)}^{0(\Phi,f)}(\mathbf{x},\mathbf{x}_r)\right\}^* + v_i^S(\mathbf{x}_r,\mathbf{x}_s)\left\{G_{(M,ij)}^{0(\Phi,h)}(\mathbf{x},\mathbf{x}_r)\right\}^*\right)n_{r,j}\,d\mathbf{x}_r \\ &-\int_{\partial V_r}\left(\tau_{ij}(\mathbf{x}_r,\mathbf{x}_s)\left\{G_{(M,i)}^{S(\Phi,f)}(\mathbf{x},\mathbf{x}_r)\right\}^* + v_i(\mathbf{x}_r,\mathbf{x}_s)\left\{G_{(M,ij)}^{S(\Phi,h)}(\mathbf{x},\mathbf{x}_r)\right\}^*\right)n_{r,j}\,d\mathbf{x}_r\end{aligned} \tag{1}$$

where the integration is performed along the closed boundary ∂V_r of receivers $\mathbf{x}_r$ (Figure 1). The integrand corresponds to the crosscorrelation between particle velocity and stress recordings v,τ (with subscripts *i*/*ij* specifying the selected component), and numerically computed backpropagation Green's functions G. Subscripts f,h represent external volume force and deformation rate sources respectively, while Φ refers to a potential and is associated with the subscript capital letter M, which can be substituted by P or S to identify that subsurface (virtual or imaging) receivers at point $\mathbf{x}$ record P or S energy. A further superscript 0/S is added to discriminate a reference/scattered wavefield from the full wavefield, respectively, where $G = G^0 + G^S$. $n_{r,j}$ is the *j*-th component of the outward-pointing normal vector to ∂V_r. Since the evaluation of such an integral expression requires and uses knowledge of particle velocity and the stress tensor at the receiver locations, we call this 'tensorial wavefield back-extrapolation'.

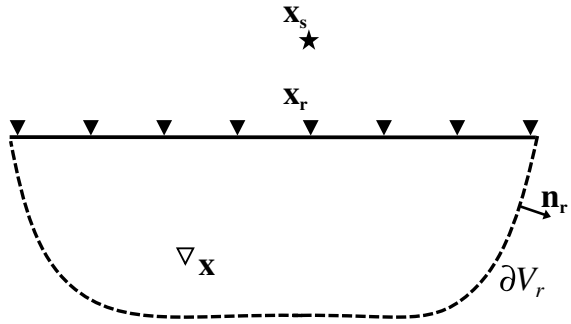

Figure 1 *Geometry used for the definition of reciprocity-based receiver wavefield back-extrapolation. A closed boundary ∂V_r of receivers surrounds a virtual receiver at the image point $\mathbf{x}$ in the subsurface, while the physical source is located outside of ∂V_r. Receivers actually used in usual acquisition scenarios are represented by triangles.*

A linearized expression suitable for reverse-time migration (so-called Born imaging) is obtained by discarding the term describing nonlinear interaction between the recorded data and the scattered backpropagators (second line of equation (1)), because it requires velocity/density models with very high spatial resolution to be computed in advance of imaging in order to obtain the G^S terms.

The main limitation is then the requirement that the stress tensor is known along the receiver boundary. In practice, when only particle velocity recordings are available they are directly injected as a boundary condition ('vectorial wavefield back-extrapolation'). This procedure can be expressed in an integral form as

$$\bar{\Phi}_M^S\left(\mathbf{x},\mathbf{x}_\mathbf{s}\right) \approx -\int_{\partial V_r} \left(v_i^S\left(\mathbf{x}_\mathbf{r},\mathbf{x}_\mathbf{s}\right)\left\{G_{(M,i)}^{0(\Phi,f)}\left(\mathbf{x},\mathbf{x}_\mathbf{r}\right)\right\}^* \right) n_{r,j}\, d\mathbf{x}_\mathbf{r} \qquad (2)$$

Such a formula is not really an approximation of the exact extrapolation integral. Rather, it is a heuristic scheme which contradicts the theory of reciprocity. Thus, in spite of being kinematically correct, it does not effectively represent the scattered Green's function between a physical source $\mathbf{x}_\mathbf{s}$ and any image point $\mathbf{x}$ at all.

Example: ERTM of a single scatterer

Consider a single point-scatterer perturbation ($\Delta\rho = 600\ kg/m^3$) embedded in a constant reference medium ($v_P = 2600\ m/s$, $v_S = 1400\ m/s$, $\rho = 1000\ kg/m^3$) at position $\mathbf{x}_{scatt} = (1000,600)m$ in the absence of a free-surface (i.e., with an absorbing boundary on the top) – Figure 1. A physical compressional source is fired at $\mathbf{x}_\mathbf{s} = (1400,50)m$ and a horizontal array of receivers is placed at $z_r = 300\,m$ with inter-receiver spacing of $\Delta x_r = 2\,m$. Both the reference wavefield and the full (reference plus scattered) field are computed using a 2D staggered grid elastic finite-difference algorithm (Virieux, 1986), and the direct arrival is subtracted from the recorded data at each receiver location to give scattered fields: $v_i^S\left(\mathbf{x}_\mathbf{r},\mathbf{x}_\mathbf{s}\right)$ and $\tau_{ij}^S\left(\mathbf{x}_\mathbf{r},\mathbf{x}_\mathbf{s}\right)$ only.

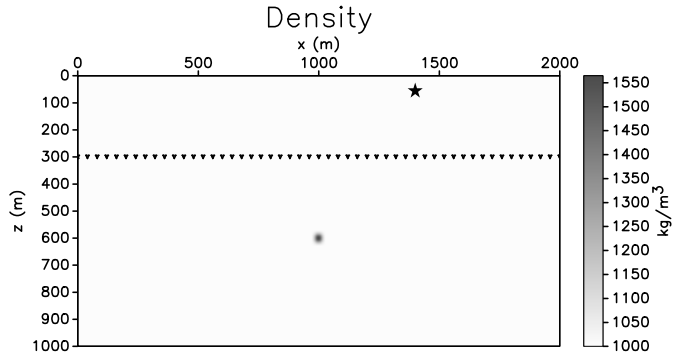

Figure 2 *Elastic reverse-time migration geometry. A single point-scatterer (black spot in the density grid) is embedded in a homogeneous medium. The star indicates the location of the physical source, and every tenth receiver is marked by a triangle.*

Figure 3 shows a snapshot at time $t = 0.34\,s$ of the estimated scattered P- and S-waves next to the modelled scattered wavefields. The left plots are obtained exactly with a full boundary of receivers plus nonlinear tensorial back-extrapolation in equation (1). The middle plots are compromised by data only being recorded on part of the receiver boundary and the use of the linearized tensorial back-extrapolation (equation (1) - without the second line). The right plots are further compromised by using the usual approximate vectorial back-extrapolation (equation (2)). Only the top side of extrapolated wavefields can be obtained because the receiver array is only available above the scatterer rather than being an enclosing array. In addition, for each arrival in the recorded data the use of only particle velocity measurements in the approximate procedure of wavefield extrapolation causes [1] joint injection of both down- and up-going waves at the receiver arrays, and [2] injection of both compressional and shear propagating modes (e.g., if a recorded P-wave is injected, both P and S propagating modes result).

The non-physical wave [2] in the estimate of the scattered P-wavefield can be explained using the stationary phase approach (Snieder et al., 2008). This highlights where, along the receiver boundary ∂V_r, the recorded data and the backpropagators interfere constructively and contribute to the creation of a wave in the receiver-side wavefield (Figure 4). Associated boundary receivers are called *stationary receivers*. Wave [2] at location $\mathbf{x}$ is caused by a P-to-S conversion recorded at $\mathbf{x}_r$ being back-propagated erroneously as a P wave from $\mathbf{x}_r$ to $\mathbf{x}$.

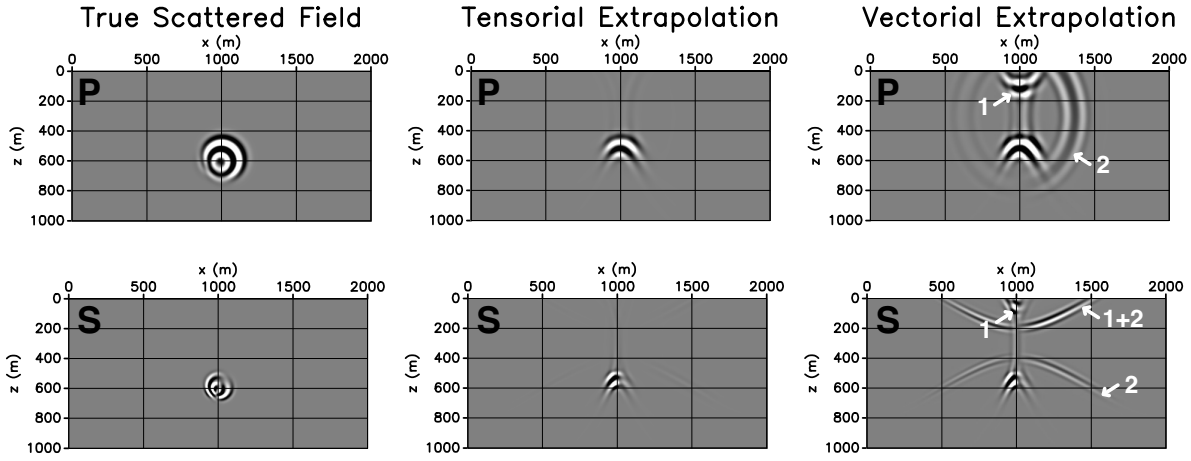

Figure 3 *P-wave (top) and S-wave (bottom) snapshots of the (left) exactly modelled, and (middle) tensorially and (right) vectorially back-extrapolated receiver-side wavefields for the point scatterer example. White arrows indicate non-physical waves due to approximations made in the vectorial wavefield extrapolation integral (equation (2)). They do not arise when the tensorial wavefield extrapolation integral is used.*

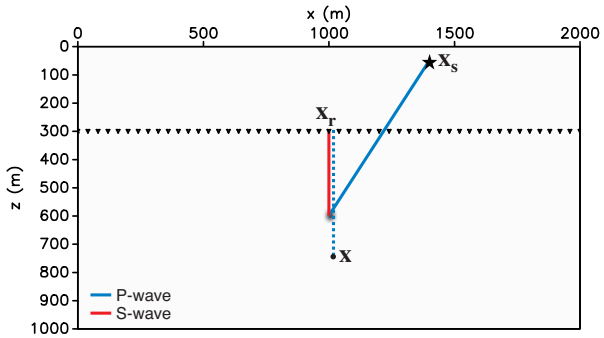

Figure 4 *Stationary phase analysis describing how the non-physical wave [2] arises at a generic image point* $\mathbf{x}$*, when the vectorial wavefield extrapolation is used to construct the scattered P-wavefield. Solid and dotted lines represent the recorded data and backpropagators, respectively. Blue lines refer to P-waves and red lines identify S-waves.*

Spurious events in receiver-side extrapolated wavefields potentially turn into artifacts in the resulting seismic images. However, since most imaging conditions use only the zero-time, zero-offset crosscorrelation between source and receiver wavefields (Claerbout, 1971), artifacts would only be created if the source-side wavefield and non-physical waves in the receiver-side wavefield coincide at an image point at a certain time.

Figure 5 shows the PP and PS images obtained from elastic reverse-time migration using either the tensorial or vectorial wavefield extrapolation, with an elastic imaging condition that crosscorrelates P- and S-wave potentials on both source and receiver sides (Yan and Sava, 2008). The scatterer is imaged in both cases, however artifacts are present when the vectorial receiver wavefield is crosscorrelated with the source wavefield (Figure 5a,c – e.g., A1 and A2 in Figure 5 caused by errors [1] and [2] in Figure 3). Since non-physical waves are suppressed in the tensorial receiver wavefield (apart from some small numerical errors), artifacts are strongly attenuated in the elastic images in Figure 5b,d, creating much clearer images which allow for a better interpretation of the subsurface structure. Moreover, by closely comparing the imaged scatterer in Figure 5b,d, we notice that its shape displays different local slopes for PP and PS images. This indicates that the angular aperture of the image at depth is different for P- and S-waves, and they could be combined to improve the result

in poorly illuminated areas.

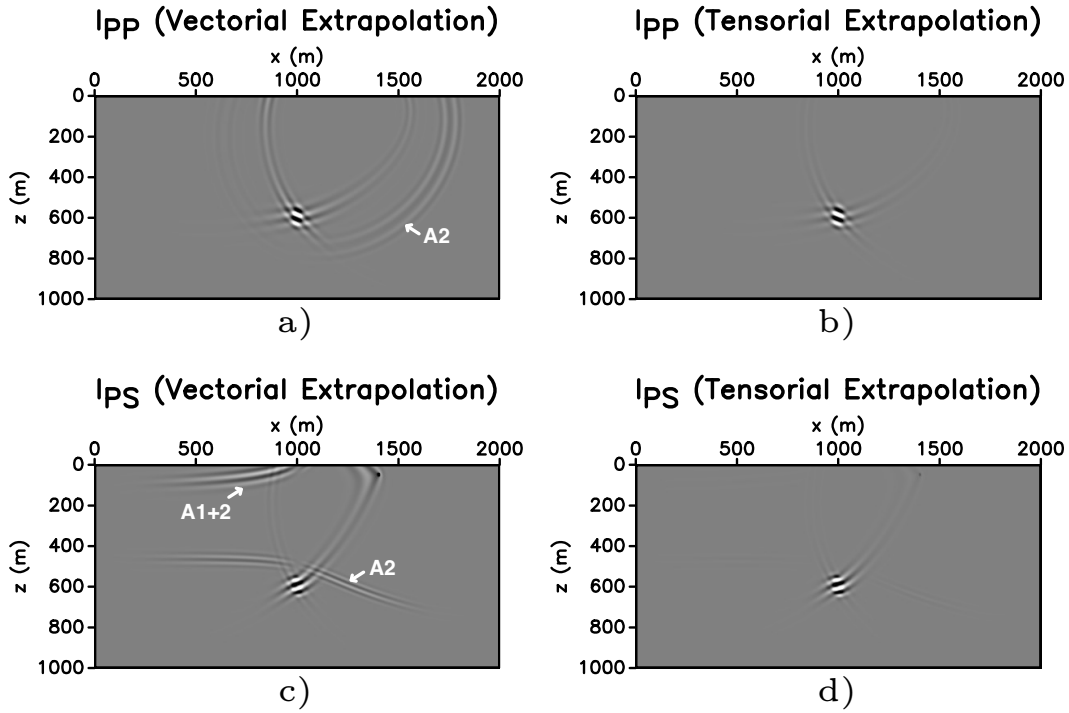

Figure 5 *PP (top) and PS (bottom) images resulting from elastic RTM using (a,c) vectorial and (b,d) tensorial wavefield extrapolation for the example in Figure 2 illuminated by a single surface source. Although the scatterer is imaged in both cases (it can not be properly localised since only a single source was used in this example), artifacts are clearly visible when only particle velocity data are injected at receiver locations during wavefield extrapolation.*

Conclusions

In this work we have derived a wavefield extrapolation formula which uses a combination of velocity-stess recordings and backpropagation sources. The receiver-side wavefields are deprived of non-physical waves that, on the contrary, arise when wavefield extrapolation is approximated by direct injection of particle velocity components at receiver locations. This leads directly to improved elastic subsurface images.

Acknowledgements

The authors thank the Edinburgh Interferometry Project (EIP) sponsors for supporting this research and granting permission to publish it. The reproducible numerical examples in this work use the Madagascar open-source package freely available from *http://www.reproducibility.org*.

References

Claerbout, J. F. [1971] Toward a unified theory of reflector mapping. Geophysics, **36**, no. 3, 467-481.

Chang, W.-F., McMechan, G. A. [1987] Elastic reverse-time migration. Geophysics, **52**, no. 10, 1365-1375.

Lu, R., Traynin, P. and Anderson, J. E. [2009] Comparison of elastic and acoustic reverse time migration on the synthetic elastic marmousi-ii obc dataset. 79th Annual International Meeting, SEG, Expanded Abstracts.

Snieder, R., van Wijk, K., Haney, M. and Calvert, R. [2008] The cancellation of spurious arrivals in Green's function extraction and the generalized optical theorem. Physical Review E, **78**, 036606.

Virieux, J. [1986] P-SV wave propagation in heterogeneous media: Velocity-stress finite-difference method. Geophysics, **51**, 889–901.

Wapenaar, K. and Fokkema, J. [2006] Green's function representations for seismic interferometry. Geophysics, **71**, SI33-SI46.

Yan, J. and Sava, P. [2008] Isotropic angle-domain elastic reverse-time migration. Geophysics, **73**, S229-S239.